

Phase selection and texturing in molybdenum oxide films grown by reactive magnetron sputtering

Faezeh A. F. Lahiji^{1,4}, Biplab Paul^{1,2}, Grzegorz Greczynski¹, Ganpati Ramanath^{1,3,4,5}, Arnaud le Febvrier⁴, Per Eklund^{1,4,5}

¹*Thin Film Physics Division, Department of Physics, Chemistry and Biology, (IFM), Linköping University, SE-58183 Linköping, Sweden*

²*PLATIT AG, Eichholzstrasse 9, 2545 Selzach, Switzerland*

³*Department of Materials Science and Engineering, Rensselaer Polytechnic Institute, Troy, NY 12180, USA*

⁴*Inorganic Chemistry, Department of Chemistry – Ångström Laboratory, Uppsala University, Box 538, SE-751 21 Uppsala, Sweden*

⁵*Wallenberg Initiative Materials Science for Sustainability, Department of Chemistry – Ångström Laboratory, Uppsala University, Box 538, SE-751 21 Uppsala, Sweden*

Abstract

Molybdenum oxide films offer a rich variety of properties for diverse applications, but exclusive synthesis of desired phases is a major challenge. Here, we demonstrate that oxygen flow ratio $f_{O_2} = [O_2]/[Ar+O_2]$ is crucial not only for phase selection of non-layered monoclinic MoO₂ and layered orthorhombic α -MoO₃ but also for controlling grain size and preferred orientation. Both mica and sapphire support exclusive MoO₂ formation in the $0.15 \leq f_{O_2} \leq 0.25$ window at deposition temperatures $T_{dep} = 400$ and 500 °C, and α -MoO₃ formation in the $0.35 < f_{O_2} \leq 0.5$ window at 400 °C. Within f_{O_2} windows favoring exclusive phase formation, high f_{O_2} fosters large grains with out-of-plane $0k0$ texture, except for MoO₂ films on c-sapphire that show no systematic trends. These findings provide a framework for rational synthesis of phase-pure monoclinic MoO₂ and orthorhombic MoO₃ with control over texture and microstructure to access desired properties.

Introduction

Molybdenum oxide thin films are attractive for a variety of applications in electro/photo-chromic coatings [1,2], resistive memories [3,4], displays [5] and gas sensing [6]. Exclusive phase selection is crucial because optoelectronic properties [7] depend on the Mo oxidation state and MoO_x stoichiometry, but is a challenge because of the rich variety of phases and polymorphs in the Mo-O system. One can obtain multiple Mo_nO_{3n-1} Magnéli phases [8,9] with $4 \leq n \leq 13$ [10] besides the monoclinic MoO₂ [8,9,11] and orthorhombic MoO₃ [1,12], all of which offer vastly different properties. For instance, MoO₂ with Mo⁴⁺ is a metallic conductor while MoO₃ with Mo⁶⁺ is an optically transparent insulator. Molybdenum oxide films can be synthesized by many methods including wet-chemical routes [13–15], spray pyrolysis [16], and chemical [17] and physical [7,18,19] vapor deposition. Reactive magnetron sputtering of a Mo target with an oxygen/argon plasma allows exclusive MoO_x phase formation by suitable choice of substrate, deposition temperature T_{dep} and oxygen flow [20] to counter the tendency to form multiple phases.

This work shows the roles of oxygen flow ratio $f_{O_2} = [O_2]/[Ar+O_2]$ and deposition temperature T_{dep} on the selective formation of monoclinic MoO₂ and orthorhombic α -MoO₃. We find that f_{O_2} influences not only phase selection, but also the grain orientation and microstructure. Exclusive formation of monoclinic MoO₂ and orthorhombic α -MoO₃ are supported at specific f_{O_2} ranges within $0.1 \leq f_{O_2} \leq 0.50$ on both mica and sapphire for T_{dep} = 400 and 500 °C. Within the exclusive phase formation windows, high f_{O_2} favors large grains and strong out-of-plane $0k0$ textures of monoclinic MoO₂ and orthorhombic α -MoO₃, compared to smaller low-textured grains at low f_{O_2} . These insights should pave the way for the exclusive synthesis of phase-selected MoO_x films with control over grain size and texture for accessing and tuning desired properties for applications.

Experimental details

Molybdenum oxide thin films were grown using pulsed dc reactive magnetron sputter deposition from a 99.99% pure 50-mm-diameter Mo target from Plasmaterials. The Mo target was powered with bipolar pulsed-dc voltage pulses at 150 W and 100 kHz with a 2 μ s reverse time and 80% duty cycle to inhibit arcing. The substrates were 10 \times 10 mm² pieces of fluorphlogopite KMg₃(AlSi₃O₁₀)F₂(001) mica --referred henceforth as f-mica-- purchased from Continental Trade, and c-plane sapphire(0001) --referred henceforth as c-sapphire-- purchased from Alineason. The

substrates were mounted on a rotatable sample holder in a 3×10^{-6} Pa base pressure UHV sputter-deposition chamber described elsewhere [21]. Immediately prior to loading, fresh f-mica surfaces were exposed by scotch-tape exfoliation. Wet-chemical treatments were eschewed to obviate solvent intercalation and vacuum degradation. The c-sapphire substrates were ultrasonicated successively in acetone and ethanol for 5 minutes each and blow-dried with N_2 .

Molybdenum oxide films were deposited by adjusting the oxygen flow ratio $f_{O_2} = [O_2]/[Ar+O_2]$ in the $0.05 \leq f_{O_2} \leq 0.50$ range. All depositions were carried out for 30 minutes at 2.5 mTorr pressure with total gas flow fixed at 60 ± 1.5 sccm. Prior to each deposition, the Mo target was sputter-cleaned at 1.7 mTorr Ar pressure at 150 W power for 2 minutes. The substrates were preheated to $T_{dep} = 400$ °C or 500 °C and held for 15 minutes for temperature homogenization.

Symmetric θ - 2θ X-ray diffraction (XRD) scans were acquired in a PANalytical X'Pert PRO diffractometer with a Cu K_α beam ($\lambda = 1.54$ Å) source operated at 45 kV and 40 mA. The incident optics include a 0.5° divergence slit, a 0.5° anti-scatter slit, and a Ni filter to minimize Cu K_β . The diffracted beam included a 5.0 mm anti-scatter slit and 0.04 rad Soller slits. The PreFIX stage, equipped with an X'Celerator detector, was set to acquire data during θ - 2θ scans with a $0.0167^\circ/\text{step}$ size and equivalent time/step of 24.76 using the PIXcel 1D detector.

Film morphology was characterized by a Leo 1550 Gemini, Zeiss scanning electron microscope (SEM) operated at 4 kV using in- and off-lens detectors to map Z-contrast and topography, respectively. X-ray Photoelectron Spectroscopy (XPS) was conducted to determine the oxidation state of Mo using a Kratos Analytical Axis Ultra DLD system with a monochromatic 1486.6 eV Al K_α source. The base pressure during measurements was 1.1×10^{-9} Torr (1.5×10^{-7} Pa). All spectra were recorded at 150 W anode power and normal emission angle. Setting a 20 eV analyzer pass energy results in a 0.55 eV full-width- half-maximum for the Ag $3d_{5/2}$ peak in a reference sample containing sputter-deposited Au, Ag, and Cu. The spectrometer calibration was verified by comparing Au $4f_{7/2}$, Ag $3d_{5/2}$ and Cu $2p_{3/2}$ positions to the recommended ISO standards for monochromatic Al K_α [22,23]. The spectra were acquired over a 0.3×0.7 mm² area and charge-referenced to the Fermi level $E_F = 0$ eV [24]. We present results recorded from samples in the as-received state.

Results and Discussion

Monoclinic MoO₂ formation at 500 °C

Diffraction patterns from molybdenum oxide films deposited on f-mica (Fig. 1a) with the lowest $f_{O_2} = 0.05$ and the highest $f_{O_2} = 0.5$ exhibit only the $00l$ f-mica substrate peaks ($4 \leq l \leq 14$), suggesting amorphous MoO_x formation. Multiple Bragg reflections from monoclinic MoO₂ [8] were detected for $0.1 \leq f_{O_2} \leq 0.35$ with relative intensities varying with f_{O_2} . For $f_{O_2} = 0.30$ and 0.35 , only the 020 and 040 MoO₂ peaks are seen, indicating that the $0k0$ planes in monoclinic MoO₂ crystals are preferentially aligned with $00l$ planes in f-mica. The lack of crystalline phase formation at high f_{O_2} is likely due to oxygen-poisoning of the Mo target [25–27].

Diffraction patterns from films on c-sapphire (Fig. 1b) show monoclinic MoO₂ formation for $0.05 \leq f_{O_2} \leq 0.25$. Outside this range, the exclusive presence of $00l$ c-sapphire reflections suggests possible amorphous MoO_x formation. For $f_{O_2} = 0.05$, only the $00l$ and $0k0$ reflections from MoO₂ are seen, suggesting exclusive phase formation. An additional peak from hexagonal MoO₂ [28] detected at $f_{O_2} = 0.1$, underscores the sensitivity of phase selection to oxygen flow. The one-dimensional phase diagram with representative interplanar spacings of MoO_x phases formed plotted versus f_{O_2} (see Fig. 1c-d) shows that monoclinic MoO₂ is exclusively favored on f-mica for $0.1 \leq f_{O_2} \leq 0.35$, and on c-sapphire for $0.05 \leq f_{O_2} \leq 0.25$. However, at $f_{O_2} = 0.1$, distinct diffraction peaks corresponding to hexagonal MoO₂ are observed.

Monoclinic MoO₂ and orthorhombic α -MoO₃ formation at 400 °C

At $T_{\text{dep}} = 400$ °C, the films grown on f-mica (Fig. 2a) at $f_{O_2} = 0.05$ show no detectable MoO_x reflections, suggesting possible amorphous MoO_x formation, reminiscent of the behavior at $T_{\text{dep}} = 500$ °C. The $0k0$, $0kl$, and $hk0$ Bragg reflections from monoclinic MoO₂ are observed for $0.1 \leq f_{O_2} \leq 0.25$, indicating exclusive phase selection. For $f_{O_2} = 0.30$, three phases are observed: monoclinic MoO₂ indicated by the $0k0$ reflections, traces of monoclinic Mo₈O₂₃ [29] specified by the $h0l$ reflection, and orthorhombic α -MoO₃ [30] indicated by hkl , $0k0$, and $h0l$ peaks. At $f_{O_2} = 0.35$, only orthorhombic α -MoO₃ peaks are detected for $0.35 < f_{O_2} \leq 0.5$.

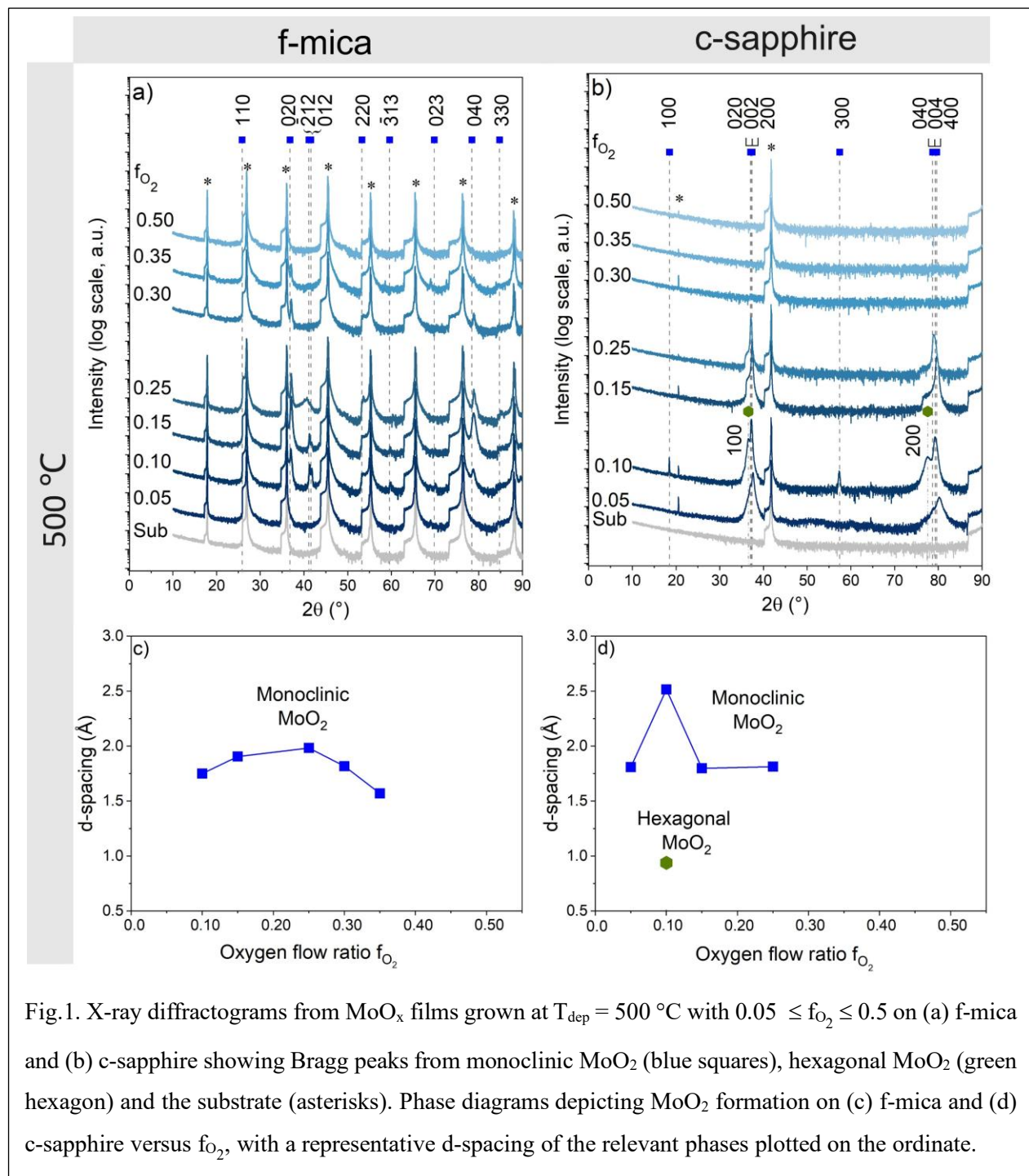


Fig.1. X-ray diffractograms from MoO_x films grown at $T_{\text{dep}} = 500 \text{ }^\circ\text{C}$ with $0.05 \leq f_{O_2} \leq 0.5$ on (a) f-mica and (b) c-sapphire showing Bragg peaks from monoclinic MoO₂ (blue squares), hexagonal MoO₂ (green hexagon) and the substrate (asterisks). Phase diagrams depicting MoO₂ formation on (c) f-mica and (d) c-sapphire versus f_{O_2} , with a representative d-spacing of the relevant phases plotted on the ordinate.

Except for minor differences, MoO_x films grown on c-sapphire at 400 °C and 500 °C show similar behaviors. For $0.05 \leq f_{O_2} \leq 0.1$, we predominantly observe $00l$ and $h00$ peaks from monoclinic MoO₂ (Fig. 2b) together with traces of $hk0$ and hkl reflections from orthorhombic

Mo₄O₁₁ [31]. At $f_{O_2} = 0.1$, we observe an additional unindexed peak at $2\theta = 76.64^\circ$ not associated with known MoO_x phases. For $0.15 < f_{O_2} \leq 0.25$, we exclusively observe monoclinic MoO₂.

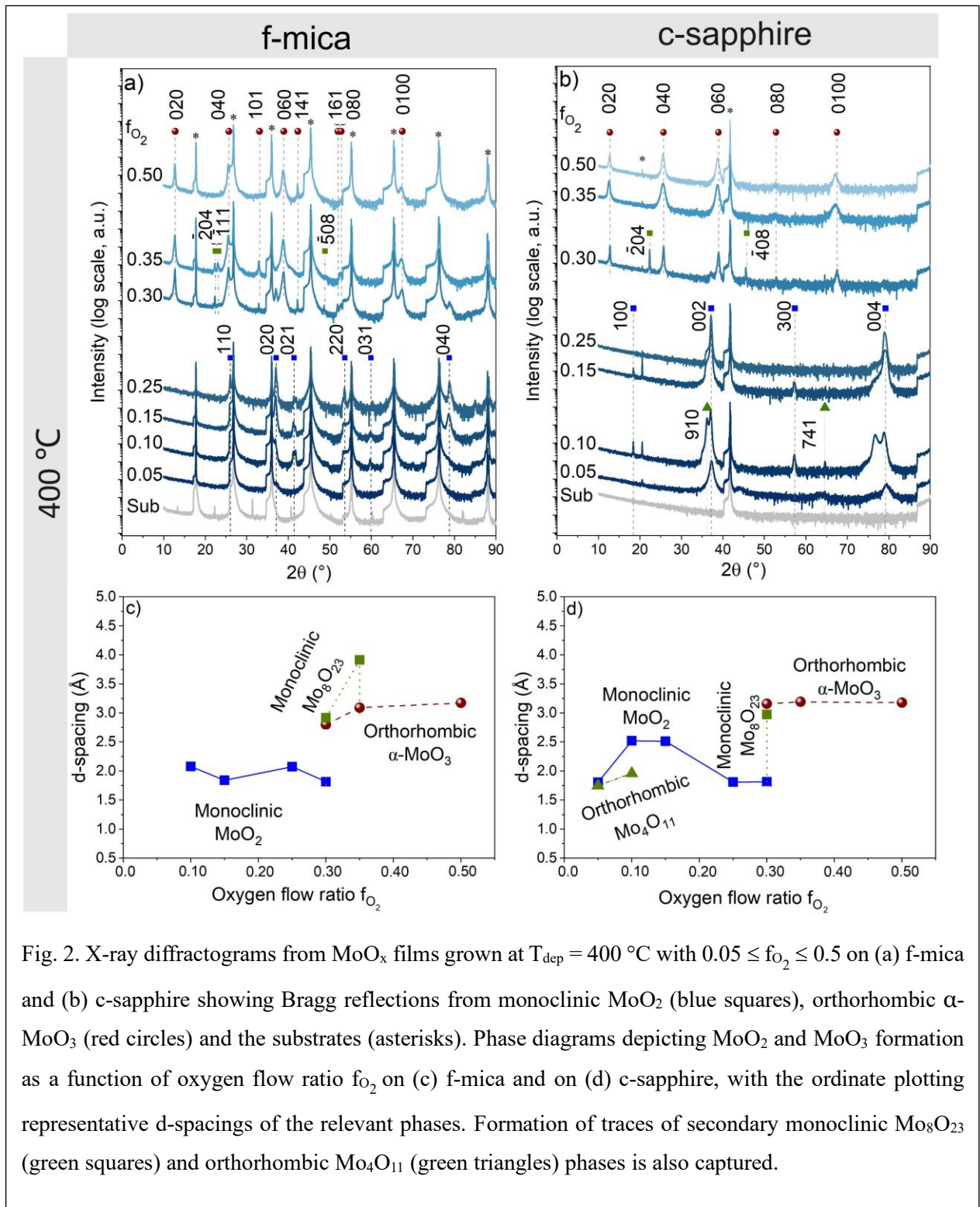


Fig. 2. X-ray diffractograms from MoO_x films grown at $T_{\text{dep}} = 400^\circ\text{C}$ with $0.05 \leq f_{O_2} \leq 0.5$ on (a) f-mica and (b) c-sapphire showing Bragg reflections from monoclinic MoO₂ (blue squares), orthorhombic α -MoO₃ (red circles) and the substrates (asterisks). Phase diagrams depicting MoO₂ and MoO₃ formation as a function of oxygen flow ratio f_{O_2} on (c) f-mica and on (d) c-sapphire, with the ordinate plotting representative d-spacings of the relevant phases. Formation of traces of secondary monoclinic Mo₈O₂₃ (green squares) and orthorhombic Mo₄O₁₁ (green triangles) phases is also captured.

At $f_{O_2} = 0.3$, orthorhombic MoO_3 and monoclinic Mo_8O_{23} are observed with traces of monoclinic MoO_2 similar to that seen on f-mica. Only orthorhombic MoO_3 forms for $0.35 \leq f_{O_2} \leq 0.5$.

XRD at 400 °C (Figs. 2c-d) indicates that MoO_2 is favored at low f_{O_2} , and α - MoO_3 is favored at high f_{O_2} , with a tendency for secondary phases at intermediate f_{O_2} . On f-mica, monoclinic MoO_2 forms exclusively at $0.1 \leq f_{O_2} \leq 0.25$ while orthorhombic α - MoO_3 is the sole phase observed at $f_{O_2} = 0.50$. Both phases form at $f_{O_2} = 0.30$, and $f_{O_2} = 0.35$ features traces of other polymorphs. On c-sapphire, exclusive monoclinic MoO_2 formation is restricted to $0.15 \leq f_{O_2} \leq 0.25$, while exclusive α - MoO_3 formation is seen for a broader range of $0.35 \leq f_{O_2} \leq 0.50$. Traces of other secondary phases are seen for $0.05 \leq f_{O_2} \leq 0.10$ and $f_{O_2} = 0.30$.

Mo-O bonding chemistry oxidation state

XPS spectra recorded from as received MoO_x films grown on f-mica and c-sapphire substrates at $T_{dep} = 400$ °C are shown in Fig. 3. Films grown at $f_{O_2} = 0.25$ exhibit prominent Mo^{+4} spin-split doublet with $3d_{5/2} - 3d_{3/2}$ peaks at 229.4 eV and 232.5, respectively on both f-mica and c-sapphire (Fig. 3a and b), consistent with monoclinic MoO_2 indicated by XRD results. Lower-intensity $3d_{5/2} - 3d_{3/2}$ doublets at 231.0 / 234.2 eV and 232.5 / 235.65 eV correspond to Mo^{+5} and Mo^{+6} oxidation states, respectively [32–34]. Since XRD results show only MoO_2 Bragg reflections at $f_{O_2} = 0.25$, these higher oxidation states may occur in the amorphous or nanocrystalline phase and/or be restricted to the surface.

Films grown on f-mica with $f_{O_2} = 0.35$ reveal nearly the exclusive presence of Mo^{+6} state (Fig. 3c-d) on f-mica and c-sapphire, indicating the MoO_3 phase, consistent with the XRD results. In particular, the Mo $3d_{5/2}/3d_{3/2}$ doublet at 232.9 / 236.0 eV which is associated with a bluish-white coloration agrees with the reported value for MoO_3 [35,36]. Additionally, the presence of Mo^{+5} oxidation state, indicated by peaks located at $231.5/234.6 \pm 0.05$ eV for $3d_{5/2}$ and $3d_{3/2}$, respectively is associated with oxygen vacancies and positively charged structural defects in MoO_3 lattice on both substrates, with a more pronounced intensity on c-sapphire [35,37] .

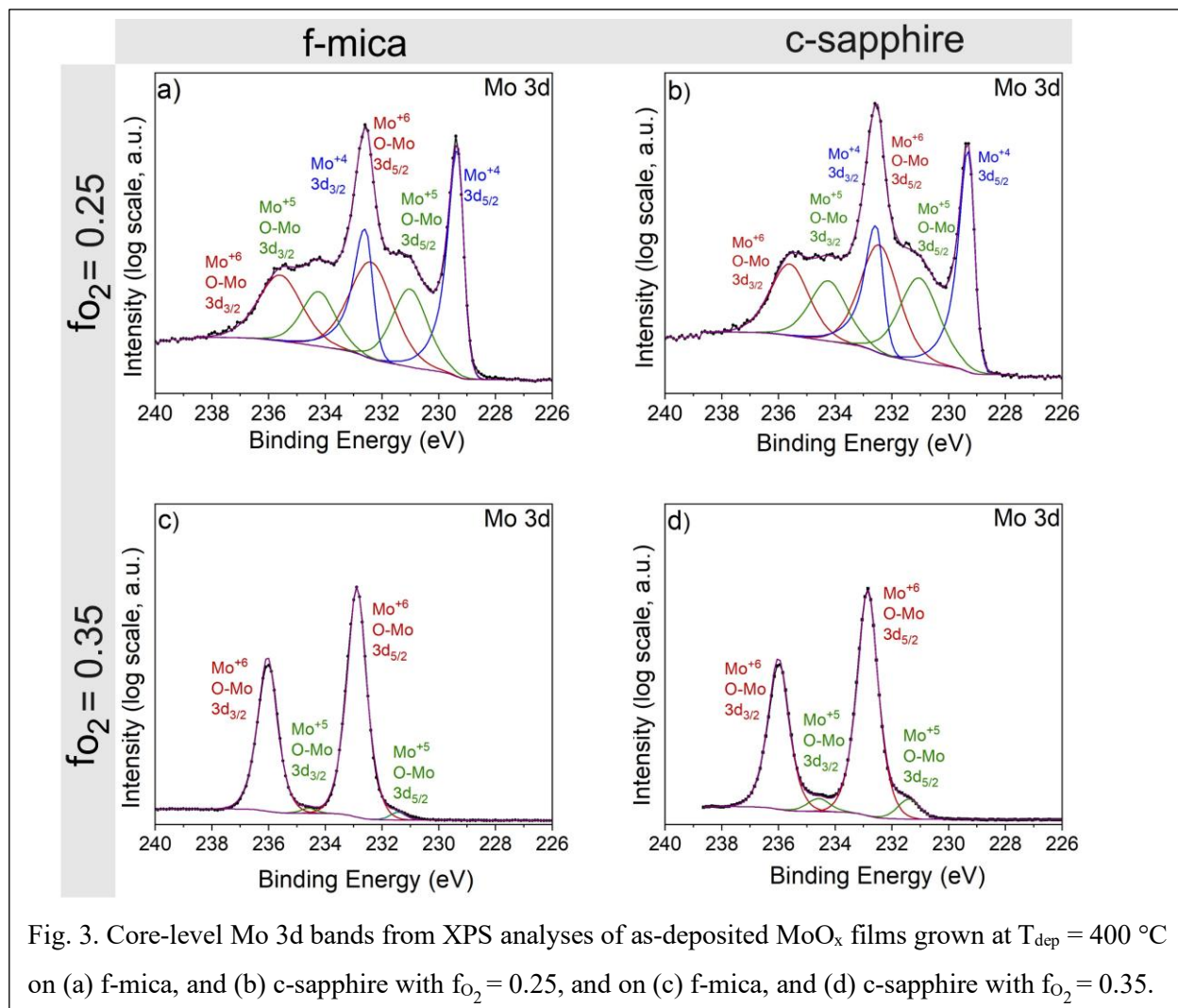


Fig. 3. Core-level Mo 3d bands from XPS analyses of as-deposited MoO_x films grown at T_{dep} = 400 °C on (a) f-mica, and (b) c-sapphire with f_{O₂} = 0.25, and on (c) f-mica, and (d) c-sapphire with f_{O₂} = 0.35.

Preferred orientation as a function of f_{O₂}

Monoclinic MoO₂ films deposited on f-mica at 500 °C show increasing out-of-plane *020* texture with increasing f_{O₂} (Fig. 4a). The non-*0k0* MoO₂ reflections of comparable intensity seen at low f_{O₂} suggest diverse grain orientations. As f_{O₂} increases, the non-*0k0* reflections decrease in number and completely disappear at f_{O₂} = 0.30 even as the *020* MoO₂ reflection intensities continue to increase with f_{O₂} for 0.30 ≤ f_{O₂} ≤ 0.35. The trends are similar for T_{dep} = 400 °C (Fig. 4b) but are somewhat obscured by the presence of additional phases. The f_{O₂}-driven accentuation of out-of-plane *020* texture indicates the tendency of *020* planes in the MoO₂ crystals align with f-mica *00l*.

MoO₂ films on c-sapphire show no T_{dep} - f_{O₂} windows with texture-f_{O₂} correlations. Films grown at T_{dep}=500 °C (Fig. 4c) feature dominant *002* MoO₂ reflections for f_{O₂}= 0.05, and f_{O₂}=0.1,

with smaller 020 MoO_2 . Higher $f_{\text{O}_2} = 0.15$, and $f_{\text{O}_2} = 0.25$, result in solitary 200 and 002 peaks, respectively. Films grown at $T_{\text{dep}} = 400$ °C (Fig. 4d) with $f_{\text{O}_2} = 0.05$ and 0.25 showing solitary 002 and 020 peaks. The 002 peak dominates over smaller 100 reflection for $f_{\text{O}_2} = 0.1$, and 0.15 .

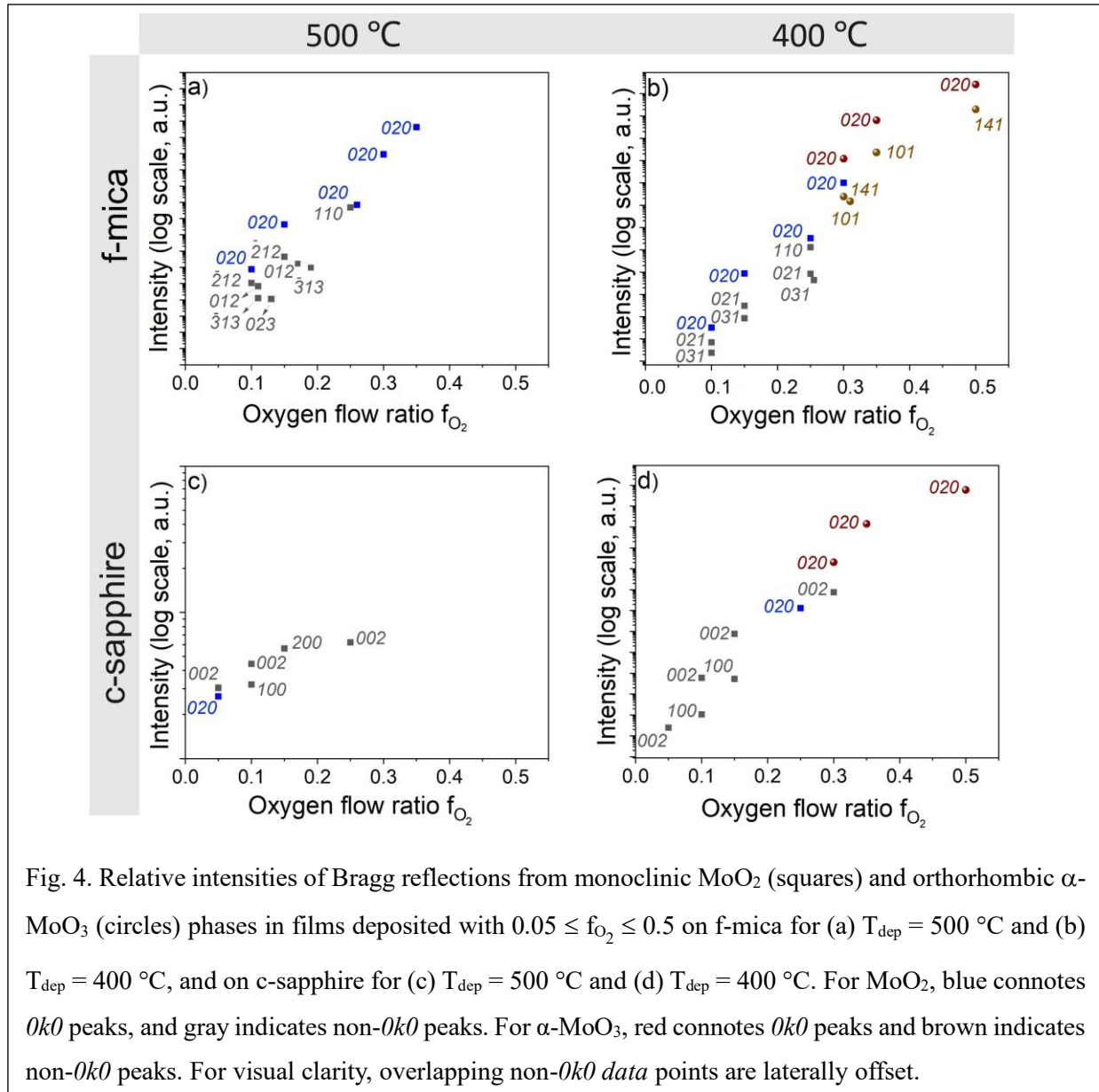


Fig. 4. Relative intensities of Bragg reflections from monoclinic MoO_2 (squares) and orthorhombic $\alpha\text{-MoO}_3$ (circles) phases in films deposited with $0.05 \leq f_{\text{O}_2} \leq 0.5$ on f-mica for (a) $T_{\text{dep}} = 500$ °C and (b) $T_{\text{dep}} = 400$ °C, and on c-sapphire for (c) $T_{\text{dep}} = 500$ °C and (d) $T_{\text{dep}} = 400$ °C. For MoO_2 , blue connotes $0k0$ peaks, and gray indicates non- $0k0$ peaks. For $\alpha\text{-MoO}_3$, red connotes $0k0$ peaks and brown indicates non- $0k0$ peaks. For visual clarity, overlapping non- $0k0$ data points are laterally offset.

Orthorhombic $\alpha\text{-MoO}_3$ films deposited with $0.30 \leq f_{\text{O}_2} \leq 0.50$ at 400 °C show a strong out-of-plane $0k0$ texture on both f-mica (Fig. 4b) and c-sapphire (Fig. 4d). Out-of-plane 020 texture indicates the tendency of the b-axis of the $\alpha\text{-MoO}_3$ crystals to orient along the surface normal of both f-mica

and c-sapphire substrates. The monotonic increase in the $0k0$ α - MoO_3 intensity for films on c-sapphire for $0.30 \leq f_{\text{O}_2} \leq 0.5$ indicates enhanced $0k0$ texturing with increasing f_{O_2} .

The above results collectively indicate that high f_{O_2} correlates with higher $0k0$ textures in MoO_2 on f-mica and MoO_3 films on both f-mica and c-sapphire for f_{O_2} - T_{dep} windows of exclusive formation of these phases. These texture- f_{O_2} correlations seen for these phase-substrate combinations are valuable for tailoring texture by adjusting f_{O_2} .

Microstructures of MoO_2 and MoO_3 films

Films exclusively containing either MoO_2 or MoO_3 phases exhibit distinctive microstructures on f-mica and c-sapphire. While the MoO_2 microstructure was sensitive to both the substrate and T_{dep} , nearly identical MoO_3 microstructures were obtained on both substrates. Monoclinic MoO_2 films on f-mica at $T_{\text{dep}} = 500$ °C and $f_{\text{O}_2} = 0.25$ reveal ~ 190 -nm-sized plate-shaped grains with ~ 25 -nm-thick plate edges-oriented outward from the surface plane (Fig. 5a). MoO_2 films on c-sapphire (Fig. 5b) show coarser anisotropic ~ 34 -nm-wide ~ 130 -nm-long prism-shaped crystals merging with each other, similar to that reported sputter-deposited MoO_2 films [38]. At $T_{\text{dep}} = 400$ °C for the same $f_{\text{O}_2} = 0.25$, MoO_2 films on both f-mica and c-sapphire exhibit similar microstructures (Figs. 5c-d) with finer grain sizes than seen at $T_{\text{dep}} = 500$ °C. In particular, the plate-shaped grains of MoO_2 on f-mica are ~ 16 -nm-wide and ~ 57 -nm-thick. The prism-shaped MoO_2 crystals c-sapphire are ~ 24 -nm-

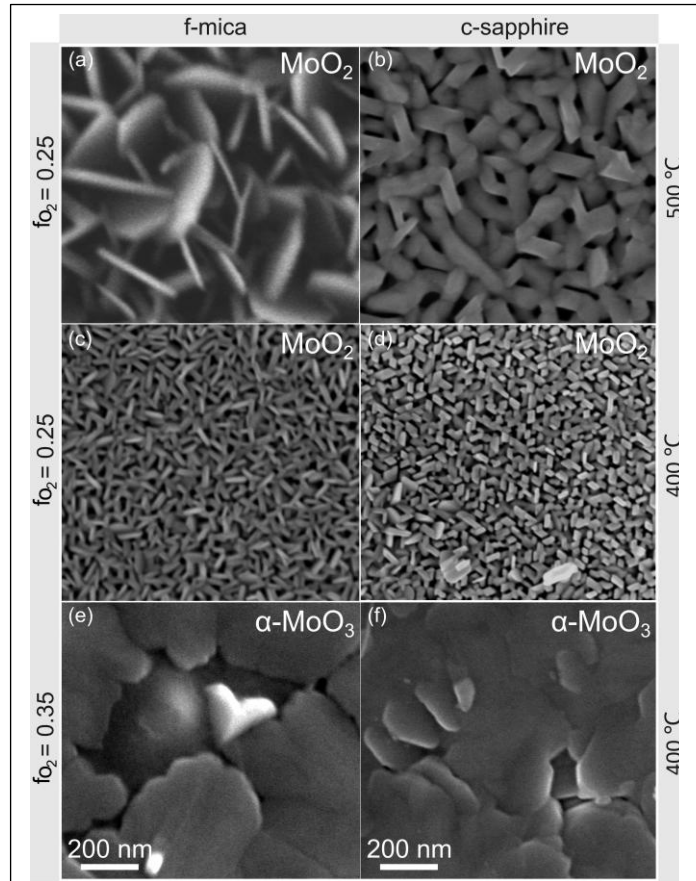


Fig. 5. SEM micrographs from films with either exclusive monoclinic MoO_2 or orthorhombic MoO_3 phases obtained at specific f_{O_2} - T_{dep} combinations on f-mica and c-sapphire.

wide and ~70-nm-long. The finer grain structure at lower T_{dep} is consistent with lower surface adatom mobilities and diffusion distances during film growth. Orthorhombic α - MoO_3 films obtained at $f_{\text{O}_2} = 0.35$ consist of large 200-600-nm-wide sheet-shaped grains on both substrates (Figs. 5e-f).

These microstructures of MoO_2 and MoO_3 featuring distinctively shaped crystals point to the connection between crystal shape and preferred orientation. For instance, the out-of-plane $0k0$ MoO_2 texture on f-mica indicates a preference for $0k0$ planes to stack along the thinnest dimension of the plate-shaped grains. The prism-shaped grains in MoO_2 films on c-sapphire correlate with the presence of prominent $h00$ and $00l$ peaks. The large flat sheets of α - MoO_3 are consistent with a strong out-of-plane $0k0$ texture on both substrates.

Conclusions

Oxygen flow ratio f_{O_2} is a key factor in determining phase selection, texture, and microstructure of MoO_x films grown on f-mica and c-sapphire by reactive magnetron sputtering. Phase-pure monoclinic MoO_2 and orthorhombic α - MoO_3 films can be exclusively obtained by adjusting f_{O_2} and the deposition temperature T_{dep} . Broadly, low f_{O_2} favors MoO_2 formation at $T_{\text{dep}} \sim 400$ and 500 °C, while high f_{O_2} favors α - MoO_3 formation at the lower temperature. Within the f_{O_2} windows of exclusive formation of MoO_2 and α - MoO_3 films, higher f_{O_2} fosters $0k0$ texture, except for MoO_2 films on c-sapphire that show no systematic trends. These findings provide a framework for synthesis of phase-pure monoclinic MoO_2 and orthorhombic MoO_3 with control over texture and microstructure.

Acknowledgements

The authors acknowledge funding from the Swedish Government Strategic Research Area in Materials Science on Functional Materials at Linköping University (Faculty Grant SFO-Mat-LiU No. 2009 00971), the Knut and Alice Wallenberg foundation through the Wallenberg Academy Fellows program (KAW-2020.0196), the Swedish Research Council (VR) under Project No. 2021-03826, and the Swedish Energy Agency under project number 52740-1. This work was partially supported by the Wallenberg Initiative Materials Science for Sustainability (WISE) funded by the Knut and Alice Wallenberg Foundation, and the US National Science Foundation grant CMMI 2135725 through the BRITE program.

References

- [1] M.R. Tubbs, MoO₃ layers — optical properties, colour centres, and holographic recording, *Phys. Stat. Sol. (a)* 21 (1974) 253–260. <https://doi.org/10.1002/pssa.2210210127>.
- [2] J. Scarminio, A. Lourenço, A. Gorenstein, Electrochromism and photochromism in amorphous molybdenum oxide films, *Thin Solid Films* 302 (1997) 66–70. [https://doi.org/10.1016/S0040-6090\(96\)09539-9](https://doi.org/10.1016/S0040-6090(96)09539-9).
- [3] A. Rasool, R. Amiruddin, I.R. Mohamed, M.C.S. Kumar, Fabrication and characterization of resistive random access memory (ReRAM) devices using molybdenum trioxide (MoO₃) as switching layer, *Superlattices and Microstructures* 147 (2020) 106682. <https://doi.org/10.1016/j.spmi.2020.106682>.
- [4] M. Arita, H. Kaji, T. Fujii, Y. Takahashi, Resistance switching properties of molybdenum oxide films, *Thin Solid Films* 520 (2012) 4762–4767. <https://doi.org/10.1016/j.tsf.2011.10.174>.
- [5] V.K. Sabhapathi, O.Md. Hussain, P.S. Reddy, K.T.R. Reddy, S. Uthanna, B.S. Naidu, P.J. Reddy, Optical absorption studies in molybdenum trioxide thin films, *Phys. Stat. Sol. (a)* 148 (1995) 167–173. <https://doi.org/10.1002/pssa.2211480114>.
- [6] D. Mutschall, K. Holzner, E. Obermeier, Sputtered molybdenum oxide thin films for NH₃ detection, *Sensors and Actuators B: Chemical* 36 (1996) 320–324. [https://doi.org/10.1016/S0925-4005\(97\)80089-5](https://doi.org/10.1016/S0925-4005(97)80089-5).
- [7] A.A. Al-Muntaser, M.A. Nasher, M.M. Makhlof, Structural, electrical, and linear/nonlinear optical characteristics of thermally evaporated molybdenum oxide thin films, *Ceramics International* 48 (2022) 8069–8080. <https://doi.org/10.1016/j.ceramint.2021.12.007>.
- [8] A. Magnéli, G. Andersson, G. Sundkvist, On the MoO₂ structure type, *Acta Chem. Scand* 9 (1955) 1378–1381.
- [9] A. MAGNÉLI, B.B.L.-H. ANSSON, L. KIHILBORG, G. SUNDKVIST, Studies on Molybdenum and Molybdenum Wolfram Oxides of the Homologous Series MenO_{3n-1}, *Acta Chem. Scand* 9 (1955).
- [10] Y. Bando, Y. Kato, T. Takada, Crystal growth of molybdenum oxides by chemical transport, *Bulletin of the Institute for Chemical Research, Kyoto University* 54 (1976) 330–334.
- [11] P. Bakhru, Equilibria between MoO₂ and liquid molybdenum oxide, (1972).
- [12] O. Concepción, O. De Melo, The versatile family of molybdenum oxides: synthesis, properties, and recent applications, *J. Phys.: Condens. Matter* 35 (2023) 143002. <https://doi.org/10.1088/1361-648X/acb24a>.
- [13] C.V. Ramana, I.B. Troitskaia, V.V. Atuchin, M. Ramos, D. Ferrer, Electron microscopy characterization of hexagonal molybdenum trioxide (MoO₃) nanorods, *Journal of Vacuum Science & Technology A: Vacuum, Surfaces, and Films* 28 (2010) 726–729. <https://doi.org/10.1116/1.3397791>.
- [14] A. Guerfi, L.H. Dao, Electrochromic Molybdenum Oxide Thin Films Prepared by Electrodeposition, *J. Electrochem. Soc.* 136 (1989) 2435–2436. <https://doi.org/10.1149/1.2097408>.
- [15] V.S. Saji, C. Lee, Molybdenum, Molybdenum Oxides, and their Electrochemistry, *ChemSusChem* 5 (2012) 1146–1161. <https://doi.org/10.1002/cssc.201100660>.
- [16] A. Bouzidi, N. Benramdane, H. Tabet-Derraz, C. Mathieu, B. Khelifa, R. Desfeux, Effect of substrate temperature on the structural and optical properties of MoO₃ thin films prepared by spray pyrolysis technique, *Materials Science and Engineering: B* 97 (2003) 5–8. [https://doi.org/10.1016/S0921-5107\(02\)00385-9](https://doi.org/10.1016/S0921-5107(02)00385-9).

- [17] N. Wazir, C. Ding, X. Wang, X. Ye, X. Lingling, T. Lu, L. Wei, B. Zou, R. Liu, Comparative Studies on Two-Dimensional (2D) Rectangular and Hexagonal Molybdenum Dioxide Nanosheets with Different Thickness, *Nanoscale Res Lett* 15 (2020) 156. <https://doi.org/10.1186/s11671-020-03386-x>.
- [18] J. Sun, Q. Zheng, S. Cheng, H. Zhou, Y. Lai, J. Yu, Comparing molybdenum oxide thin films prepared by magnetron sputtering and thermal evaporation applied in organic solar cells, *J Mater Sci: Mater Electron* 27 (2016) 3245–3249. <https://doi.org/10.1007/s10854-015-4151-4>.
- [19] M. Bivour, F. Zähringer, P. Ndione, M. Hermle, Sputter-deposited WO_x and MoO_x for hole selective contacts, *Energy Procedia* 124 (2017) 400–405. <https://doi.org/10.1016/j.egypro.2017.09.259>.
- [20] V. Bhosle, A. Tiwari, J. Narayan, Epitaxial growth and properties of MoO_x ($2 < x < 2.75$) films, *Journal of Applied Physics* 97 (2005) 083539. <https://doi.org/10.1063/1.1868852>.
- [21] A. Le Febvrier, L. Landälv, T. Liersch, D. Sandmark, P. Sandström, P. Eklund, An upgraded ultra-high vacuum magnetron-sputtering system for high-versatility and software-controlled deposition, *Vacuum* 187 (2021) 110137. <https://doi.org/10.1016/j.vacuum.2021.110137>.
- [22] M. Seah, Summary of ISO/TC 201 Standard: VII ISO 15472: 2001—surface chemical analysis—x-ray photoelectron spectrometers—calibration of energy scales, *Surface and Interface Analysis: An International Journal Devoted to the Development and Application of Techniques for the Analysis of Surfaces, Interfaces and Thin Films* 31 (2001) 721–723.
- [23] I. ISO, 15472: 2010 Surface chemical analysis—X-ray photoelectron spectrometers—calibration of energy scales, ISO: Geneva, Switzerland (2010).
- [24] G. Greczynski, L. Hultman, Binding energy referencing in X-ray photoelectron spectroscopy, *Nature Reviews Materials* (2024) 1–17.
- [25] Sook Oh M, Seob Yang B, Ho Lee J, Ha Oh S, Soo Lee U, Jang Kim Y, Joon Kim H, Soo Huh M. Improvement of electrical and optical properties of molybdenum oxide thin films by ultralow pressure sputtering method. *Journal of Vacuum Science & Technology A*. 2012 May 1;30(3)., (2024).
- [26] Fernandes Cauduro AL, Fabrim ZE, Ahmadpour M, Fichtner PF, Hassing S, Rubahn HG, Madsen M. Tuning the optoelectronic properties of amorphous MoO_x films by reactive sputtering. *Applied Physics Letters*. 2015 May 18;106(20)., (2024).
- [27] S. Mohamed, O. Kappertz, J. Ngaruiya, T.L. Pedersen, R. Drese, M. Wuttig, Correlation between structure, stress and optical properties in direct current sputtered molybdenum oxide films, *Thin Solid Films* 429 (2003) 135–143.
- [28] J.A. Kaduk, MAXIMIZING THE IMPACT OF YOUR DATA: APPLICATIONS OF RIETVELD ANALYSIS TO INDUSTRIAL PROBLEM SOLVING, (1999).
- [29] H. Fujishita, M. Sato, S. Sato, S. Hoshino, Structure determination of low-dimensional conductor Mo₈O₂₃, *Journal of Solid State Chemistry* 66 (1987) 40–46. [https://doi.org/10.1016/0022-4596\(87\)90218-0](https://doi.org/10.1016/0022-4596(87)90218-0).
- [30] T. Leisegang, A. Levin, J. Walter, D. Meyer, In situ X-ray analysis of MoO₃ reduction, *Crystal Research and Technology: Journal of Experimental and Industrial Crystallography* 40 (2005) 95–105.
- [31] H.-K. Fun, P. Yang, M. Sasaki, M. Inoue, H. Kadomatsu, γ -Mo₄O₁₁, *Acta Crystallographica Section C* 55 (1999) 841–843. <https://doi.org/10.1107/S0108270199000165>.
- [32] J.-G. Choi, L. Thompson, XPS study of as-prepared and reduced molybdenum oxides, *Applied Surface Science* 93 (1996) 143–149.

- [33] D.O. Scanlon, G.W. Watson, D. Payne, G. Atkinson, R. Egdell, D. Law, Theoretical and experimental study of the electronic structures of MoO₃ and MoO₂, *The Journal of Physical Chemistry C* 114 (2010) 4636–4645.
- [34] H. Liu, X. Tian, Y. Liu, H.A. Munir, W. Hu, X. Fan, X. Liu, L. Pang, Synergistic Polysulfides Adsorption–Conversion with Mo₂C–MoO₂ Heterostructure for Kinetically Enhanced Lithium–Sulfur Battery, *Energy Technology* 12 (2024) 2300820.
- [35] M. Anwar, C. Hogarth, R. Bulpett, Effect of substrate temperature and film thickness on the surface structure of some thin amorphous films of MoO₃ studied by X-ray photoelectron spectroscopy (ESCA), *Journal of Materials Science* 24 (1989) 3087–3090.
- [36] L. Firment, A. Ferretti, Stoichiometric and oxygen deficient MoO₃ (010) surfaces, *Surface Science* 129 (1983) 155–176.
- [37] D. Sheng, M. Zhang, X. Wang, S. Zhou, S. Fu, X. Liu, Q. Zhang, Carbon nanotubes embedded in α -MoO₃ nanoribbons for enhanced lithium-ion storage, *Journal of Materials Science: Materials in Electronics* 33 (2022) 11743–11752.
- [38] O. De Melo, V. Torres-Costa, Y. González, A. Ruediger, C. De Melo, J. Ghanbaja, D. Horwat, A. Escobosa, O. Concepción, G. Santana, E. Ramos, Interfacial strain defines the self-organization of epitaxial MoO₂ flakes and porous films on sapphire: experiments and modelling, *Applied Surface Science* 514 (2020) 145875. <https://doi.org/10.1016/j.apsusc.2020.145875>.